Stabilizer disentangling of conformal field theories

M. Frau[1][†], P. S. Tarabunga[2, 3, 4], M. Collura[1, 5], E. Tirrito[4, 6] and M. Dalmonte[4]

1 International School for Advanced Studies (SISSA), Via Bonomea 265, I-34136 Trieste, Italy
2 Technical University of Munich, TUM School of Natural Sciences, Physics Department, 85748 Garching, Germany
3 Munich Center for Quantum Science and Technology (MCQST), Schellingstr. 4, 80799 München, Germany
4 The Abdus Salam International Centre for Theoretical Physics (ICTP), Strada Costiera 11, 34151 Trieste, Italy
5 INFN, Sezione di Trieste, Via Valerio 2, 34127 Trieste, Italy
6 Dipartimento di Fisica "E. Pancini", Università di Napoli "Federico II", Monte S. Angelo, 80126 Napoli, Italy

† mfrau@sissa.it

Abstract

Understanding how entanglement can be reduced through simple operations is crucial for both classical and quantum algorithms. We investigate the entanglement properties of lattice models hosting conformal field theories cooled via local Clifford operations, a procedure we refer to as stabilizer disentangling. We uncover two distinct regimes: a constant gain regime, where disentangling is volume-independent, and a log-gain regime, where disentanglement increases with volume, characterized by a reduced effective central charge. In both cases, disentangling efficiency correlates with the target state magic, with larger magic leading to more effective cooling. The dichotomy between the two cases stems from mutual stabilizer Renyi entropy, which influences the entanglement cooling process. We provide an analytical understanding of such effect in the context of cluster Ising models, that feature disentangling global Clifford operations. Our findings indicate that matrix product states possess subclasses based on the relationship between entanglement and magic, and clarifying the potential of new classes of variational states embedding Clifford dynamics within matrix product states.

1   Introduction

Building on the revolutionary concept of formulating the renormalization group based on eigenvalues of reduced density matrices [1], tensor network (TN) states [2–8] have found widespread applications in the context of many-body theory. One key aspect of such class of variational state is that their limiting factor, entanglement, is very well understood, so that it is possible to exploit this fact for controlled computations. Over the years, there has been a growing interest in expanding the representation power of tensor network states, by dressing their structure with additional operations that could cope with such a limiting resource. One of the earliest examples along this line is the multi-entanglement renormalization ansatz [9], where layers of additional generic entangling gates provide the entangling power. More recent examples are augmented tree tensor networks (TTN) [10, 11] and augmented matrix product states (MPS) [12]. The basic idea behind the identification of larger basins of variational states is that one feeds a controlled amount of entanglement by dressing input states via (entangling) two-body operations. While very powerful in principle, such generic dressing of tensor networks often incurs in considerable computational overheads, and does not lend itself to simple physical interpretations in terms of which classes of states can be accessed.

   A sharply different approach has been put forward recently, merging entanglement with another fundamental proxy of quantum complexity originating from quantum error correction - non-stabilizerness, also known as magic [13–15]. The basic idea is to dress tensor network
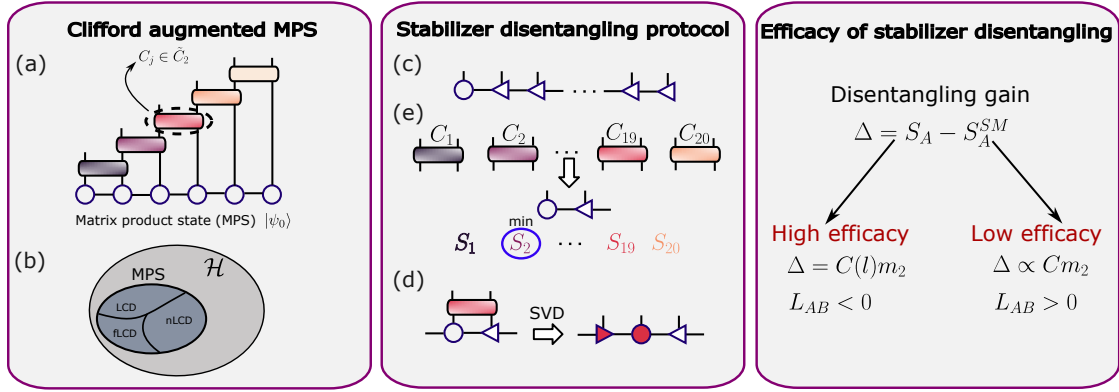
Figure 1: **a-b**: Clifford augmented MPS. **(a)**: schematics of a single sweep of local stabilizer disentangling protocol applied onto a matrix product state (MPS); **(b)**: Hilbert space structure of many-body steates for a spin system. The manifold comprising MPS can be further split with respect to how much they can be disentangled by local Clifford: local-Clifford disentanglable (LCD; disentangling improves with size), non local-Clifford disentanglable (nLCD; disentangling does not improve with size), and fully disentanglable (fLCD). In the text, we elaborate examples of all three cases: tricritical Ising point, XXZ critical, and cluster Ising model. **c-e**: Illustration of the Stabilizer disentangling protocol (see Sec.3.1). **(c)**: Obtain the groundstate with DMRG and bring it to a right-normalized form; **(d)** Apply the gates in $\tilde{\mathcal{C}}_2$ (see 3.1) to the first bond, selecting the gate that minimizes the entanglement entropy on that bond; **(e)** Apply the chosen gate to the MPS, perform a Singular Value Decomposition, update the first two tensors in the MPS, and repeat step (d) on the next bond.

[49] states not with generic operations, but rather, with a restricted class of gates harvested from
[50] the Clifford group: in one-dimension, the corresponding variational class goes under the name
[51] of Clifford augmented matrix product states (CAMPS) [16] or Stabiliser TN [17] (as well as the
[52] corresponding dressed operators [18]), that have been proposed inspired by the observation of
[53] strong relationship between entanglement and magic in both random [19] and ground matrix
[54] product states [20]. As far as the Clifford-dressing operation keeps a local structure, the new
[55] ansatz allows to extend computations straightforwardly and, at the same time, to represent
[56] states with arbitrary entanglement with modest computational resources, as demonstrated
[57] within several algorithmic instances [16, 21–23]. The limiting factor of such approach is how
[58] can one represent a state at fixed magic, while lowering entanglement with strictly local op-
[59] erations. Understanding the descriptive power of such Clifford-augmented TN raises a deep
[60] question in terms of the entanglement/magic interplay in many-body states, that is, how can
[61] we actually "cool" their entanglement properties via application of stabilizer gates that are
[62] local in nature.

[63] Here, we study the question whether one-dimensional conformal field theories [24] can be
[64] entanglement-cooled via local stabilizer operations. Such theories represent an ideal testing
[65] ground to understand the nature of stabilizer disentangling, as they combine a fundamental
[66] theoretical relevance, with a mild, logarithmic violation of the area law [25, 26]. Starting from
[67] the matrix-product state representation of ground states of spin chains, we apply a Clifford
[68] circuit whose structure is made of local two-body gates. In order to comply with the structure
[69] of MPS, the basic protocol we follow is a sweeping procedure, schematically illustrated in
[70] Fig. 1a, where each two-body gate is harvested from the Clifford group on nearest-neighbors.

[71] We find that the Hilbert space of lattice conformal field theories features three distinct
[72] classes, depending on how effectively local stabilizer operators disentanglement works (see

Fig. 1b). The first class is made of states whose entanglement can only be lowered by a constant: we deem those states non local-Clifford disentanglable (nLCD). The second class comprises states whose entanglement can be systematically cooled as size increases: the effective description of such systems is via a effective central charge, that is smaller with respect to the target state one. We define these staes are local-Clifford disentanglable (LCD). Finally, some states can be perfectly disentangled, at least for specific partitions, via local Clifford - we deem those fully LCD (fLCD).

Local stabilizer cooling depends very strongly on the original state properties. Firstly, we show how, for all cases, the total amount of magic is related (and, at time, directly proportional) to entanglement cooling efficacy. We argue how such - in principle, very unexpected - finding can be justified based on the very special correlation structure of ground states, that is at odds with that of random Haar states. Secondly, we show how the efficacy of local stabilizer cooling with respect to size is dictated by the mutual stabilizer Renyi entropy (mSRE) [27–29]. This quantity is akin to mutual information in the context of Renyi entropies, and describes how spread in stabilizer space a given partition is. States for which mSRE is negative are those where stabilizer disentangling improves with size, while for those with positive mSRE, no improvement is observed. We elucidate this fact via extensive numerical computations, and analytical understanding via exactly soluble cluster-Ising models [30].

Our results thus show how, within the Hilbert space corner described by matrix product states, there is fundamental a difference between states that can be disentangled by Clifford operations, and states that cannot (see Fig. 1). This emphasises the potential for CAMPS to describe efficiently a broader class of phenomena with respect to MPS, with emphasis on states with vanishing non-local magic content.

The rest of the paper is structured as follows. In Sec. 2, we review the concept of magic, introduce the main observables we target, and review how those are computed in tensor network states. In Sec. 3, we describe the local entanglement cooling protocol, and show how CAMPS can be dramatically simplified. Sec. 4, we review the models we investigate numerically, while in Sec. 5, we discuss the corresponding numerical results. The origin of efficient stabilizer disentangling is then elaborated upon in Sec. 6, investigating cluster Ising models. Finally, we draw our conclusions and present a detail outlook of our findings in the broader context of augmented tensor network states.

2 Basics of Magic

2.1 Definition

Magic quantifies the extent to which a quantum state deviates from the class of stabilizer states, a subset of quantum states that can be efficiently simulated on classical computers. In this section, we briefly review the key definitions necessary for their characterization.

Consider a system of N qbits, with Hilbert space $\mathcal{H} = \otimes_{j=1}^{N} \mathcal{H}_i$. The Pauli group $\mathcal{P}_N$ is defined as

$$\mathcal{P}_N = \left\{ e^{i\theta\frac{\pi}{2}} \sigma_{j_1} \otimes \cdots \sigma_{j_N} | \theta, j_k = 0, 1, 2, 3 \right\}. \tag{1}$$

It includes all operator strings composed of tensor products of N Pauli operators, each multiplied by a phase factor of ± 1 or $\pm i$.

The stabilizer group $\mathcal{S}$ of a N-qubits pure quantum state $|\psi\rangle$ is an abelian subgroup of $\mathcal{P}_N$ and contains all the strings that stabilize the state, namely

$$S|\psi\rangle = |\psi\rangle, \quad \forall S \in \mathcal{S}. \tag{2}$$

115 A state is a stabilizer states if $|\mathcal{S}| = 2^N$. Such a state can be efficiently simulated via stabilizer
116 formalism [31]. Alternatively, a stabilizer state can be described in terms of the resources
117 required for its preparation. The Clifford group of N qbits $\mathcal{C}_N$ consists of unitary operators that
118 serve as the normalizer of $\mathcal{P}_N$, mapping a Pauli string in another Pauli string via conjugaiton,
119 specifically

$$\mathcal{C}_N = \left\{ U \text{ such that } UPU^\dagger \in \mathcal{P}_N \text{ for all } P \in \mathcal{P}_N \right\}. \tag{3}$$

120 It is generated by the Hadamard gate, the $\frac{\pi}{4}$ and the CNOT gate. It is well-known that Clifford
121 group alone is insufficient for universal quantum computation [14], and must be supplemented
122 by the T gate. Stabilizer state are those states that can be prepared by means of only Clifford
123 operations, starting from a product state $|0\rangle^{\otimes N}$.

124   Magic represents the deviation from the set of stabilizer states, reflecting the amount
125 of non-Clifford resources required for state preparation. For this reason, the properties re-
126 quired for a good measure of magic, that we denote as $\mathcal{M}$, are the following:(i) Faithfullness:
127 $\mathcal{M}(|\psi\rangle) = 0$ iff $|\psi\rangle$ is a stabilizer state (ii) Invariance under Clifford unitaries: $\mathcal{M}(\Gamma|\psi\rangle) \leq \mathcal{M}(|\psi\rangle)$,
128 for $\Gamma \in \mathcal{C}_N$, and (iii) Additivity: $\mathcal{M}(|\psi\rangle \otimes |\phi\rangle) = \mathcal{M}(|\psi\rangle) + \mathcal{M}(|\phi\rangle)$ (in general, sub-additivity
129 is sufficient). Several measures that meet these criteria have been proposed in quantum in-
130 formation theory, including the min-relative entropy of magic [32], the relative entropy of
131 nonstabilizerness [13], the robustness of magic [32, 33], the stabilizer rank, stabilizer ex-
132 tend [34], mana, thauma (for qudit) [35], stabilizer nullity [36], CSS entropy [37], and the
133 basis-minimized stabilizerness asymmetry [38]. However, many of these measures involve
134 complex minimization procedures, which complicate their computation in many-body systems.
135 To face the problem of computability, more practical measures of nonstabilizerness have been
136 recently introduced, including Bell magic [39] and stabilizer Rényi entropies (SREs) [27].
137 Unfortunately, their calculation still requires evaluating an exponential number of terms. Nev-
138 ertheless, notable progress has been made in their experimental measurements [40–43] and
139 large-scale numerical simulations [28, 29, 44–48].

2.2 Full-state magic

141 In this study, we measure magic using SREs [27]. For a pure quantum state of N qubits ρ,
142 SREs are defined as

$$M_n(\rho) = \frac{1}{1-n} \log \left\{ \sum_{P \in \tilde{\mathcal{P}}_N} \frac{\mathrm{Tr}(\rho P)^{2n}}{2^N} \right\}, \tag{4}$$

143 where P is a Pauli string and $\tilde{\mathcal{P}}_N$ is the projective Pauli group, namely the standard Pauli group
144 modulo the global phases. This definition satisfies properties (i), (ii) and (iii) mentioned
145 in the previous section. Eq. 4 coincides with the n-Rényi entropy associated to the classical
146 probability distribution

$$\Xi_P = \frac{\mathrm{Tr}(\rho P)^2}{2^N} \tag{5}$$

147 Magic generally scales linearly with the system size N. Therefore, in the following, we will
148 consider the SRE density defined as $m_n = M_n/N$. The SREs provide useful measures for
149 evaluating the total magic content of a quantum state. However, for the purpose of this work
150 — specifically, assessing the effectiveness of the Stabilizer Disentangling Algorithm — metrics
151 beyond the total magic of the full state are needed.

2.3 Mutual Stabilizer Renyi entropy

We can extend the definition of SRE to mixed states, namely when $\text{Tr}(\rho^2) \neq 1$, by properly normalizing the above probability,

$$\tilde{\Xi}_P = \frac{\text{Tr}(\rho P)^2}{2^N \text{Tr}(\rho^2)} \tag{6}$$

such that we still have $\sum_P \tilde{\Xi}_P = 1$. For example, for the case of Rényi index $n = 2$, the SRE of a mixed state reads

$$\tilde{M}_2 = -\log\left(\frac{\sum_{P \in P_N} |\text{Tr}(\rho P)|^4}{\sum_{P \in P_N} |\text{Tr}(\rho P)|^2} \right). \tag{7}$$

With this extension, we define the mutual SRE as

$$L_n(\rho_{AB}) = \tilde{M}_n(\rho_{AB}) - \tilde{M}_n(\rho_B) - \tilde{M}_n(\rho_A) \tag{8}$$

This quantity, reminiscent of mutual information, was first introduced in Ref. [29], and subsequently investigated in [20, 49–51]. It is worth noting that, similar to mutual Rényi entropies, $L_n(\rho_{AB})$ is not necessarily strictly positive in general.

2.3.1 Interpretation of mutual SRE

It is important to note that, very much like Renyi mutual information in the context of entanglement (which is not positive definite), the mutual SRE entropy cannot be interpreted as a generic information measure, as the reduced density matrices ρ_A, ρ_B are in general mixed. It is however very indicative of correlations, as already demonstrated in the context of quantum phase transitions, and again, in a similar manner as Renyi mutual information for entanglement.

We would like now to provide two arguments to justify its physical relevance, that will also be instrumental in interpreting the results presented below.

Spreading of information over Pauli strings. - The first perspective we would like to offer is based on the fact that SRE can be thought of as participation entropy in the Pauli basis [46, 52]. This interpretation remains correct even in cases where SRE is not a measure of magic, for instance for mixed states.

The mSRE can then be thought of as follows: if positive, this indicates that the sum of the two partitions is actually more widely spread in stabilizer subspace with respect to the original partitions (taking into account the normalization factor at the denominator in Eq. (6)). Oppositely, if negative, it implies that there is some common stabilizer states the sum of the two partitions projects onto, so as to induce a specific form of correlations between them. In the context of stabilizer disentangling, the presence of such correlation will be related to a more efficient disentangling procedure: this may be expected based on the fact that, once the circuit has sufficiently large support to capture both A and B, there is an additional degree of freedom/non-separability that can be taken care of solely via stabilizer operations.

We can have a qualitative understanding of the above argument in a simplified scenario. Suppose that there is a single stabilizer operator commuting with the state ρ, and with support on both A and B. Then, we expect a negative (albeit small due to normalization) mSRE. We will see that this is exactly what happens in cluster Ising models, where the presence of such 'hidden' encoded qubit makes stabilizer disentangling extremely efficient.

188   **Density matrix decomposition. -**   The second argument is based on the fact that any mixed
189   state on two disconnected partitions A and B can be written as follow

$$\rho_{AB} = \frac{1}{2^{N_B}}\rho_A I_B + \frac{1}{2^{N_A}} I_A \rho_B - \frac{1}{2^N} I_A I_B + \varrho_{AB} \tag{9}$$

190   where the term proportional to the identity accounts for the correct normalization of the full
191   operator, and we have $|A| = N_A$, $|B| = N_B$, $N_A + N_B = N$. The previous equation implicitly
192   defines the last term ϱ_{AB} which incorporates all contributions coming from Pauli strings which
193   have nontrivial support in both subsystems A and B. As a consequence, $\text{Tr}(\varrho_{AB}) = 0$. In
194   particular, when this term is absent, it is easy to see that the SREs of AB reduces to a particular
195   combination of the SREs of A and B separately. In fact, assuming $\varrho_{AB} = 0$ one gets for example
196   (for $n = 2$)

$$\text{Tr}(P\rho_{AB})^4 = \delta_{P_B I_B}\text{Tr}(P_A \rho_A)^4 + \delta_{P_A I_A}\text{Tr}(P_B \rho_B)^4 - \delta_{PI}, \tag{10}$$

197   where $P = P_A P_B$ with $P_A (P_B)$ is acting in the subsystem $A(B)$ only. It follows that all Pauli strings
198   with non-trivial support in both A and B have vanishing expectation values. As a qualitative
199   consequence, the mutual SRE would be particularly sensible to the absence/presence in the
200   full density matrix ρ_{AB}, of Pauli correlations acting non-trivially in A and B. In fact, after sub-
201   tracting from $L_2(\rho_{AB})$ the entanglement contribution (namely the Rényi-2 mutual information
202   $I(\rho_{AB})$), the remaining "magic" part $W(\rho_{AB})$ (see Eq.(12)) strongly depends on ϱ_{AB}.

2.4   Magic that can be removed by local operations

204   Another useful observable that we will consider below attempts to quantify the magic that a
205   given state has if restricted to a limited bond dimension description. This quantity is related
206   to the portion of magic that can be removed by applying only local operations on the state.
207   While the detailed reasoning behind introducing this quantity, that we denote as $m_2^{\chi=2}$, will be
208   thoroughly discussed in Sec. 2.5, we anticipate an intuitive explanation of this measure here:
209   $m_2^{\chi=2}(|\psi\rangle)$ represents the magic of the state closest (in L_2 norm) to $|\psi\rangle$ among those that
210   exhibit low entanglement. If the magic is primarily derived from the correlations we will get
211   $m_2^{\chi=2} \ll m_2$. Conversely, if $m_2^{\chi=2} \sim m_2$, this indicates that most of the state's magic content
212   is not due to correlations and can therefore be eliminated through local operations. In this
213   scenario, we would expect the Stabilizer Disentangling Protocol to be more effective.

2.5   Numerical Computation

215   Our computations are all based on MPSs, the simplest class of Tensor Network states, a very
216   established and powerful tool to describe groundstates of $1D$ spin-chains [53]. A pure quantum
217   state $|\psi\rangle$, in its MPS reperesentation, reads

$$|\psi\rangle = \sum_{s_1, s_2, \cdots, s_L} A^{s_1} A^{s_2} \cdots A^{s_L} |s_1, s_2, \cdots s_L\rangle \tag{11}$$

218   where A^{s_i} are $\chi \times \chi$, except for the boundaries $i = 1$, $i = L$, where the corresponding tensors
219   are, respectively, a row and a column vector of length χ. The parameter χ is the *bond dimension*
220   of the MPS and it's directly related to the entanglement of $|\psi\rangle$.
221   By utilizing this representation of the state and incorporating sampling techniques within
222   the space of the Pauli strings, we can efficiently derive the magic observables defined ear-
223   lier. Indeed, while computations for generic states typically scale exponentially with N, this
224   framework allows us to reduce the computational complexity to a linear scaling with respect
225   to system size L and number of samples N_S, and polynomial in the bond dimension χ.

Specifically, for full state magic density m_n we exploit perfect Pauli sampling, a method based on Tensor Networks perfect sampling algorithms [54, 55], and introduced for the computation of magic in Ref. [44, 45]. We employ the same technique also for the computation of $m_2^{\chi=2}$. In this case, we first variationally project the MPS $|\psi\rangle$ onto the manifold of $\chi = 2$ MPSs, and then repeat the computation.

One of the limitations of Perfect Pauli sampling is that it does not allow for computation mutual SRE between two disconnected partitions A, B as in Eq. 8. To obtain $L_n(\rho_{AB})$ we employ the Pauli-Markov sampling method introduced in Ref. [29]. In particular, we focus on the case $n = 2$, from now on denoted just $L(\rho_{AB})$, and rewrite $L(\rho_{AB})$ as

$$L(\rho_{AB}) = I(\rho_{AB}) - W(\rho_{AB}) \tag{12}$$

where $I(\rho_{AB}) = S_2(\rho_A) + S_2(\rho_B) - S_2(\rho_{AB})$ is the Rényi-2 mutual information, and

$$W(\rho_{AB}) = -\log\left(\frac{\sum_{P_A \in \mathcal{P}_A} |\mathrm{Tr}(\rho_A P_A)|^4 \sum_{P \in \mathcal{P}_B} |\mathrm{Tr}(\rho_B P_B)|^4}{\sum_{P_{AB} \in \mathcal{P}_{AB}} |\mathrm{Tr}(\rho_{AB} P_{AB})|^4} \right).$$

Each of the two terms in Eq. 12 can be sampled via a Markov-chain approach, as detailed in Ref. [29].

3 Stabilizer Disentangling via Clifford

3.1 Stabilizer disentangling protocol

We perform a disentangling procedure on a given ground state, previously obtained via standard DMRG, using a Clifford circuit consisting of two-qubits Clifford operations. The basic steps of the algorithm are depicted in Fig. 1c-e, and can be listed as follows:

(i) given the target Hamiltonian H, we run a DMRG simulation to obtain the ground state Ψ in MPS form;

(ii) we apply all possible two-qubit gates on the bond $(1, 2)$, obtaining the (unnormalized) states $|\Psi[C_1]\rangle = C_{1,2}|\psi\rangle$;

(iii) based on their bipartite entanglement entropy at the cut $(1, 2)$, we select the lowest entangled state within the set of all $|\Psi[C_1]\rangle$; we denote this state as $|\Psi[C_1^m]\rangle$, and the corresponding minimizing gate as $C_{1,2}^m$;

(iv) we repeat operations (ii-iii) sequentially for all bonds, until one obtains the CAMPS:

$$|\Psi[C_{1;L-1}]\rangle = \prod_{j=1}^{L-1} C_{j,j+1}|\psi\rangle \tag{13}$$

whose entanglement is smaller than Ψ;

(v) repeat (ii-iv) until convergence with the number of sweeps.

The resulting CAMPS will have the structure as shown in Fig. 1a. By construction, the MPS part of the CAMPS will have a systematically lower entanglement entropy compared to the MPS representation of the initial state. Note that, because of the circuit structure, the circuit becomes global after just one sweep with $O(N)$ gates. Namely, a local operator can be transformed to an operator with support on an extensive number of qubits. This is different from, e.g., brickwork circuit, where $O(N)$ depth and $O(N^2)$ gates are required.

259 **Optimized search.** - In the original CAMPS proposal [16], the full set of two-qbits Clifford
260 gates (a part from phase factors) comprising 700+ gates was used. Here, we propose a largely
261 optimized search. Let $\mathcal{C}_2$ denote the original set of two-qubit gates and $\mathcal{C}_1$ denote the set
262 of single-qubit Clifford gates. The key observation is that if two unitaries $U, V \in \mathcal{C}_2$ can be
263 expressed as $U = (S_1 \otimes S_2)V$, where $S_1, S_2 \in \mathcal{C}_1$, then U and V will have identical effects on
264 the singular values. Therefore, the search for disentangling can be restricted to a subset of $\mathcal{C}_2$,
265 that we denote $\tilde{\mathcal{C}}_2$, consisting of $|\mathcal{C}_2|/|\mathcal{C}_1 \otimes \mathcal{C}_1| = 20$ gates.

3.2 Entropy gain Δ

267 To evaluate the representational capacity of Clifford-augmented tensor networks, it is essential
268 to define an observable that quantifies the efficiency of the Stabilizer disentangling protocol.
269 We refer to this observable as entropy gain. For a subregion A of size ℓ, it is defined as

$$\Delta = S_A - S_A^{SM} . \tag{14}$$

270 Here, S_A denotes the entanglement entropy of the original state $|\Psi\rangle$, while $S_A^{(SM)}$ represents the
271 entanglement entropy of the resulting state after applying the stabilizer disentangling protocol,
272 specifically

$$S_A^{(SM)} = -\mathrm{Tr}\rho_A^{(SM)} \ln \rho_A^{(SM)},$$

273 where $\rho_A^{(SM)} = \mathrm{Tr}_{\bar{A}}|\Psi[C_{\ell;L-\ell}]\rangle\langle\Psi[C_{\ell;L-\ell}]|$ is the reduced density matrix of the final state, with
274 the trace taken over the complement of subregion A. We will refer to $S_A^{(SM)}$ as Stabilizer Mini-
275 mized Entanglement Entropy (SMEE).

4 Models

277 In this section we provide a summary of the properties of one-dimensional models employed
278 to explore stabilizer disentangling. For each of the following models, we obtain the MPS
279 approximation of the ground state at a specified bond dimension, χ, by performing Density
280 Matrix Renormalization Group (DMRG) simulations using the iTensor package [56, 57]. We
281 made sure that the results have converged in the bond dimension, so that the MPS is a faithful
282 representation of the ground state. Subsequently, we apply the techniques described in the
283 previous section to calculate the quantities of interest from the MPS.
284 Our focus in the following will be on critical spin chains governed by conformal field theory,
285 where the entanglement entropy is known to exhibit the scaling behavior [26, 58]

$$S_A = \frac{c}{6} \log\left[\frac{2L}{\pi}\sin(\ell\frac{\pi}{L})\right] + \gamma \tag{15}$$

286 in open chains. Here, ℓ denotes the subsystem size, L is the total size, c is the central charge
287 of the conformal field theory, and γ is a non-universal constant. The scaling behavior above
288 implies that a polynomial growth of bond dimension χ with L is necessary for an MPS to
289 faithfully represent the state. In the following we will examine how the stabilizer disentangling
290 procedure affects the CFT entanglement scaling.

4.1 XXZ model

292 We consider a spin-$\frac{1}{2}$ XXZ chain with open boundary conditions, described by the Hamiltonian:

$$H = -\sum_{i=1}^{L-1}\left(S_i^x S_{i+1}^x + S_i^y S_{i+1}^y + J_z S_i^z S_{i+1}^z\right) \tag{16}$$

where $S_i^\alpha = \frac{1}{2}\sigma_i^\alpha$ and σ_i^α are the Pauli matrices (with $\alpha = x, y, z$). J_z is the parameter that represents the strength of the uniaxial anisotropy along the z-direction.

The model exhibits three distinct phases [59]: A gapped ferromagnet for $J_z > 1$; a Tomonaga-Luttinger liquid phase, characterized by a CFT with a central charge $c = 1$ in the interval $|J_z| < 1$; A gapped antiferromagnet for $J_z < -1$. For $|J_z| = 1$ the model becomes equivalent to the Heisenberg model (After rotation along z when $J_z = -1$). In what follows, we will consider groundstates of this model inside the critical phase.

4.2 Tricritical Ising model

We also examine a quantum spin chain with a tricritical Ising point, as first introduced in Ref. [60]. The Hamiltonian for this model is $\mathbb{Z}_2$ symmetric and is given by:

$$H = H_I + \lambda H_T \tag{17}$$

where H_I represents the transverse field Ising model hamiltonian at the critical point $h = 1$, specifically

$$H_I = -\sum_{i=1}^{L-1} S_i^z S_{i+1}^z - \sum_{i=1}^{L} S_i^x \,, \tag{18}$$

and H_T describes a three-spins interaction term:

$$H_T = \sum_{i=1}^{L-2} \left(S_i^x S_{i+1}^z S_{i+2}^z + S_i^z S_{i+1}^z S_{i+2}^x \right) . \tag{19}$$

The model remains in the Ising universality class for $0 \leq \lambda < \lambda_{\text{TCI}}$, with a tricritical Ising (TCI) point at $\lambda_{\text{TCI}} = 0.428$, marking the transition between the critical Ising phase and a gapped phase. In the gapped phase, a $\mathbb{Z}_2$ symmetry-preserving ground state coexists with two symmetry-broken ground states. In the following, we focus on the TCI point in the phase diagram, which is described by a conformal field theory with central charge $c = 7/10$.

4.3 Cluster Ising models

Finally, we consider a class of models known as Cluster Ising models [30, 61–63], focusing on three distinct scenarios with corresponding Hamiltonians H_1, H_2, and H_3. The first Hamiltonian is defined as follows

$$H_1 = -\sum_{i=1}^{L-2} (S_i^x S_{i+1}^z S_{i+2}^x) + h \sum_{i=1}^{L} S_i^z \,. \tag{20}$$

Using a Jordan-Wigner transformation, Ref. [63] demonstrates that the model exhibits a phase transition at $h = 1$. For $h = 0$, the system's four-fold degenerate ground state (in case of open boundary conditions) is the cluster state, an example of symmetry-protected topologically ordered state, protected by a $\mathbb{Z}_2 \times \mathbb{Z}_2$ symmetry, which has been extensively studied as a resource for quantum computation [64, 65].

Expanding on this model, we introduce an additional nearest-neighbor interaction, weighted by the parameter D, as shown in the following Hamiltonian

$$H_2 = H_1 + D \sum_{i=1}^{L-1} S_i^z S_{i+1}^z \,. \tag{21}$$

Details of our computation of the critical points for this model can be found in Appendix B. Our estimate for the critical point at $D = 0.1$ yield $h_c \simeq 0.9$.

324   In both the previous cases, the critical points of the phase diagram are described by a
325   Conformal Field theory with central charge $c = 1$.
326   The third and last scenario we examine, presented in detail in Ref. [30], is the following:

$$H_3 = -\sum_{i=1}^{L-2}(S_i^x S_{i+1}^z S_{i+2}^x) + V\sum_{i=1}^{L-1} S_i^y S_{i+1}^y . \tag{22}$$

327   The phase diagram closely resembles that of the previous Cluster Ising model considered in
328   this section. In fact, for $V = 0$, the two models coincide. The model host two phases: a
329   cluster phase for $V < 1$, where multipartite entanglement is maximum, and, for $V > 1$, an
330   antiferromagnetic phase, marked by nonvanishing staggered magnetization along the y-axis
331   and a pronounced reduction in multipartite entanglement. At $V = 1$, the critical behavior of
332   the model is described by a conformal field theory with central charge $c = 3/2$.

5 Results

334   To explore the relationship between properties of different states and the efficacy of Stabilizer
335   Disentangling, we apply the stabilizer disentangling protocol in Sec.3.1 to various ground
336   states. We then compute the magic observables defined in Sec.2 to examine correlations be-
337   tween the magic content of each state and its disentanglability.
338   In studying the representational power of TNs for many-body states, a key factor is the
339   scaling of entanglement entropy with system size. It is well known that a MPS can efficiently
340   approximate the ground state of a finite spin chain with L sites when the entanglement en-
341   tropy S_A of a partition A (comprising half the chain) is bounded by $S_A \leq c \log(L/2)$ [66]. To
342   understand the impact of the Stabilizer Disentangling protocol on this bound, we analyze the
343   size scaling of both entanglement entropy and SMEE.
344   We present the results organized by model: in Sec. 5.1 we analyze the XXZ model, and in
345   Sec. 5.2 the Tricritical Ising model. In these cases, we observed that convergence showed no
346   dependence on the number of sweeps: a single sweep was sufficient to achieve the minimum
347   SMEE.

5.1 XXZ model

349   Ref. [67] demonstrates that Clifford circuits augmented with T-gates can be fully disentangled
350   through Stabilizer Cooling, provided that the number of T-gates remains below the system
351   size, L. The authors also delucidates that in the context of Hamiltonian dynamics, the behav-
352   ior differs: even at low magic density, states exhibit resistance to stabilizer disentanglement,
353   meaning they cannot be fully disentangled.
354   Our findings for the critical groundstates of the XXZ model align with those results: these
355   states cannot be disentangled completely, as shown in Fig. 3. However, we also found a new
356   characteristic specific to Stabilizer disentangling of groundstates. Fig. 2 presents the entropy
357   gain, Δ, along with various magic observables within the critical phase of the XXZ model, with
358   a fixed system size of $L = 32$. Interestingly, in Fig. 2a, we observe that

$$\Delta \sim C\, m_2 \tag{23}$$

359   where C is a proportionality constant dependent on system size, but not on the model's pa-
360   rameters.
361   Fig. 3 presents the results for the size scalings. In Fig.s 3a, 3b we observe the expected
362   logarithmic scaling of entanglement entropy within the critical phase [26]. Specifically, Fig. 3a
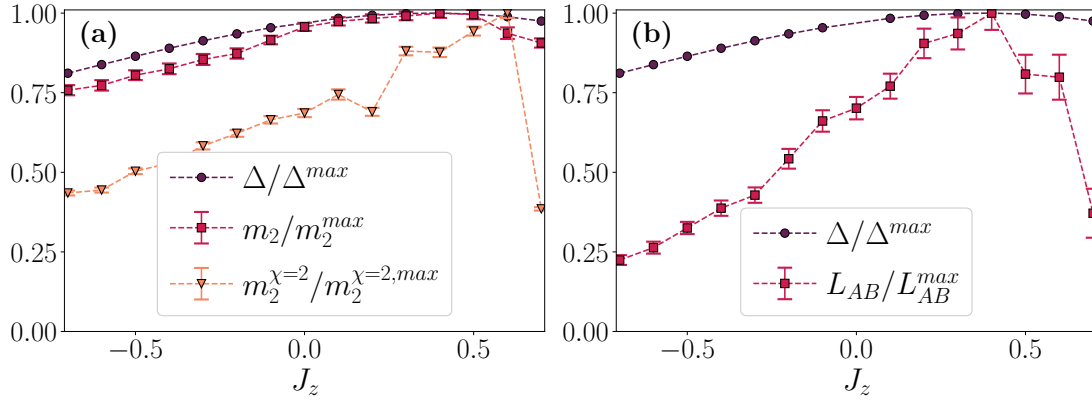
Figure 2: Entropy gain Δ compared with magic observables in the ground states of the XXZ chain across various J_z values within the critical phase, for a system size $L = 32$. The data are presented on a relative scale, with each panel scaled as follows: **(a)**: $\Delta_{\max} = 0.67$, $m_2^{\max} = 0.27$, $m_2^{\chi=2,\max} = 0.30$; **(b)**: $\Delta_{\max} = 0.67$, $|L_{AB}^{\max}| = 0.27$. **(a)** Comparison with the full state SRE density m_2 and the local magic $m_2^{\chi=2}$. The computation of m_2 and $m_2^{\chi=2}$ is performed via perfect Pauli sampling with $N_S = 10^3$ samples. **(b)** Comparison with mSRE L_{AB} where A, B are two partitions located at the boundary of the chain, each of length $\ell_A = \ell_B = L/4$. The computation of L_{AB} is performed via Pauli-Markov sampling with $N_S = 10^4$ samples.

shows the scaling of S_A for a fixed system size L of $L = 512$ as the size ℓ of the partition A varies. The x-axis is rescaled as $\log(\frac{2L}{\pi} \sin(\frac{\pi l}{L}))$. The dashed line in the figure corresponds to the linear fit: $S_A = a_1 \log(\frac{2L}{\pi} \sin(\frac{\pi l}{L})) + b_1$ (see Eq. (15)). The value of the central charge c_1 estimated using the relation $a_1 = \frac{c_1}{6}$ is found to be $c_1 = 1.016 \pm 0.001$. Figure 3b, on the other hand, displays the entanglement entropy S_A calculated fixing the size of partition A at $l = \frac{L}{2}$ and varying the size of the system L. In this case, the x-axis is rescaled as $\log(\frac{L}{\pi})$, and the central charge estimated by the fit $S_A = a_2 \log(\frac{L}{\pi}) + a_2$ (represented by the dashed line) is $c_2 = 1.015 \pm 0.001$. Both c_1 and c_2 are compatible with the central charge of the model that is $c = 1$.

In Fig. 3, we also present the results for the SMEE. As shown in Fig. 3a and Fig. 3b, the SMEE also follows the expected logarithmic trend, but appears lowered by a constant factor. Indeed, in Fig. 3c and 3d, where we illustrate the scaling of entropy gain Δ with system size, we observe that it scales sublogarithmically. Additionally, in both cases, the range of the y-axis is sufficiently narrow to be considered nearly constant, suggesting that the factor C in Eq. 24 shows no size dependence in this context. We refer to states in which Stabilizer disentangling does not improve with increasing system size as non-Local Clifford Disentanglable (nLCD) states, since the gain Δ becomes negligible in the large-L limit. As previously discussed, this behavior is not governed by the full-state magic density m_2; instead, it is associated with the state's non-local magic content. To illustrate this fact, in Fig. 2, we consider $m_2^{\chi=2}$, which represents the amount of magic that cannot be eliminated by local operations. The latter is systematically smaller than m_2. This indicates that the magic primarily originates from the correlations within the state, making it more challenging to remove entanglement through stabilizer operations.
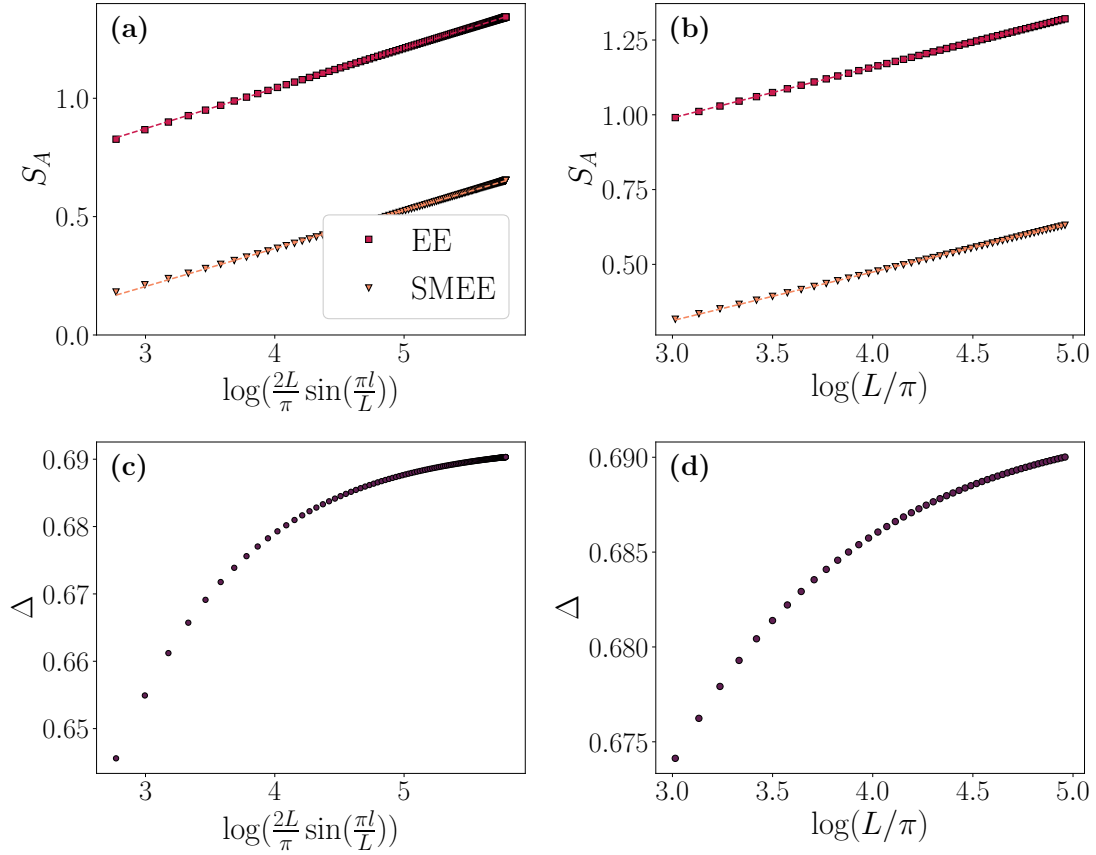
Figure 3: Stabilizer disentangling within the crical phase in XXZ model. For **(a)**, **(c)** data are shown for a fixes length of the system $L = 512$, varying the size of the partitions A, B ($\ell_A = l$, $\ell_B = L - l$) from $l = 8$ to $l = 256$. For **(b)**, **(d)** data are presented for varying total system lengths L with fixed, equally sized partitions A and B (where $\ell_A = \ell_B = L/2$). **(a)**, **(b)**: Scaling of Entanglement Entropy (EE) and Stabilizer-Minimized Entanglement Entropy (SMEE). Dashed lines represent the fitted curves, with both curves sharing the same slope. **(c)**, **(d)** Scaling of entropy gain Δ. It exhibits sublogarithmic scaling; however, due to the very small scale on the y-axis, it can effectively be considered saturated.

5.2 Tricritical Ising Model

We now move to the Tricritical Ising Model. In Fig. 4, we present the comparison between the entropy gain Δ and the various magic observables throughout the phase diagram. Consistent with the results for the XXZ model, we find a correlation between the entropy gain, Δ, and the full state magic density, m_2, for both system sizes $L = 64$ (in Fig. 4a) and $L = 128$ (in Fig. 4b). Specifically, we find

$$\Delta \sim C \, m_2 \, . \tag{24}$$

What distinguishes this scenario from the previous one is the size scaling of EE and SMEE at the Tricritical Ising point $\lambda_{\text{TCI}} = 0.428$, as illustrated in Fig. 5. In Fig.s 5a, 5b we observe that, when fixing the system size at $L = 512$ and varying the partition size ℓ, or alternatively, fixing $\ell = \frac{L}{2}$ and varying L, both size scalings exhibit the expected logarithmic behavior. Specifically, the central charges obtained by the linear fits with the functional forms $S_A = a_1 \, \log(\frac{2L}{\pi} \sin(\frac{\pi l}{L})) + b_1$ and $S_A = a_2 \, \log(\frac{L}{\pi}) + b_2$ are $c_1 = 0.705 \pm 0.003$ and
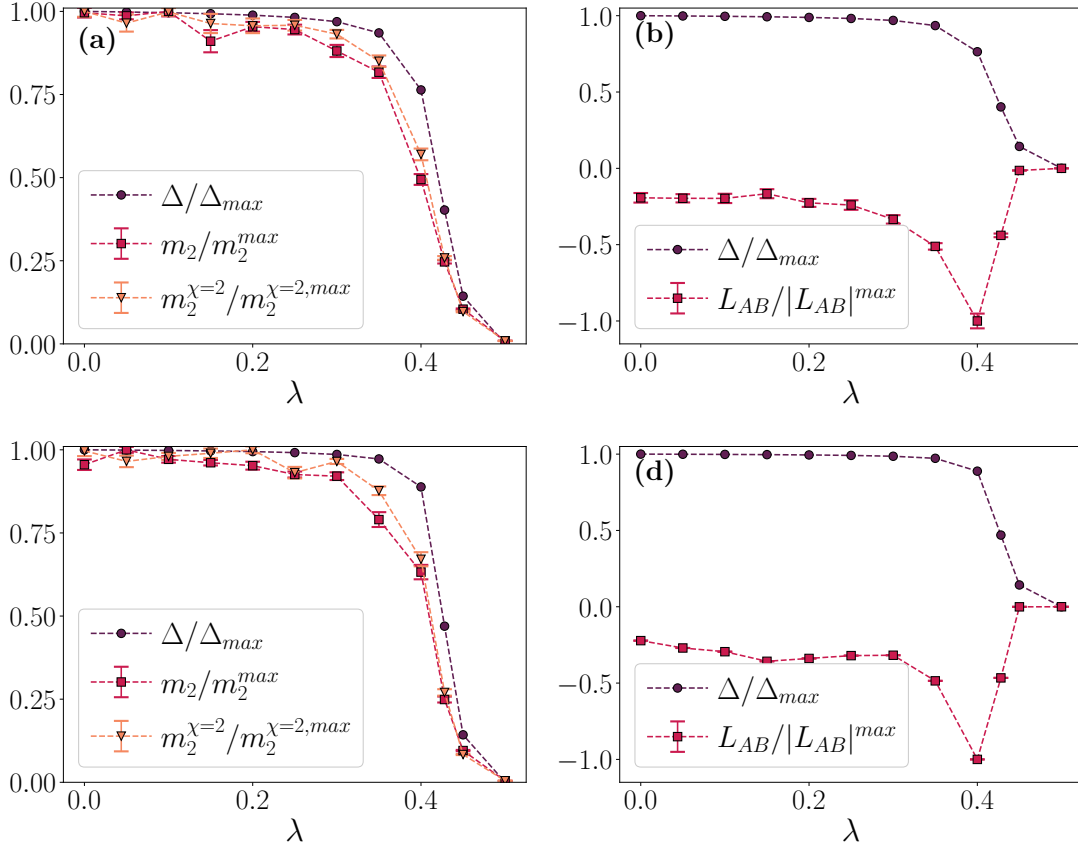
Figure 4: Entropy gain Δ compared with magic observables in the ground states of the Tricritical Ising model across various J_z values, for two system sizes: $L = 64$ (**(a)** and **(b)**) and $L = 128$ (**(c)** and **(d)**). The data are presented on a relative scale, with each panel scaled as follows: **(a)**: $\Delta_{\max} = 0.34$, $m_2^{\max} = 0.29$, $m_2^{\chi=2,\max} = 0.29$; **(b)**: $\Delta_{\max} = 0.34$, $|L_{AB}^{\max}| = 0.003$; **(c)**: $\Delta_{\max} = 0.34$, $m_2^{\max} = 0.31$, $m_2^{\chi=2,\max} = 0.31$; **(d)**: $\Delta_{\max} = 0.34$, $|L_{AB}^{\max}| = 0.002$. **(a)**, **(c)**: Comparison with the full state SRE density m_2 and the local magic $m_2^{\chi=2}$. The computation of m_2 and $m_2^{\chi=2}$ is performed via perfect Pauli sampling with $N_S = 10^3$ samples. **(b)**, **(d)**: Comparison with mSRE L_{AB} where A, B are two partitions located at the boundary of the chain, each of length $\ell_A = \ell_B = L/4$. The computation of L_{AB} is performed via Pauli-Markov sampling with $N_S = 10^4$ samples.

$c_2 = 0.736 \pm 0.005$, respectively, both of which are consistent with the central charge of the Tricritical Ising point, $c = 0.7$.

Most importantly, at odds with what happens for the XXZ model, we observe that SMEEs are not only shifted of a constant factor - they indeed show a logarithmic growth with a small prefactor. The estimated slope values are $a_1 = 0.086 \pm 0.001$ (from Fig. 5a) and $a_2 = 0.091 \pm 0.001$ (from Fig. 5b). This fact suggests that the Stabilizer disentanglement is able to map the model onto a different one, characterized by a smaller effective central charge c^{SM}. This behavior is further illustrated in Fig. 5c and Fig. 5d, where the logarithmic scaling of Δ with size is evident. The prefactors, determined by the fits (represented by the dashed lines) with the functional forms $\Delta = a_1^\Delta \log(\frac{2L}{\pi} \sin(\frac{\pi l}{L})) + b_1^\Delta$ for Fig. 5c and $\Delta = a_2^\Delta \log(\frac{L}{\pi}) + b_2^\Delta$ Fig. 5d, are $a_1^\Delta = a_2^\Delta = 0.03$, which correspond to a significant fraction of the central charge $c = 0.7$. We refer to conformal field theories for which Δ shows logarithmic scaling with sys-
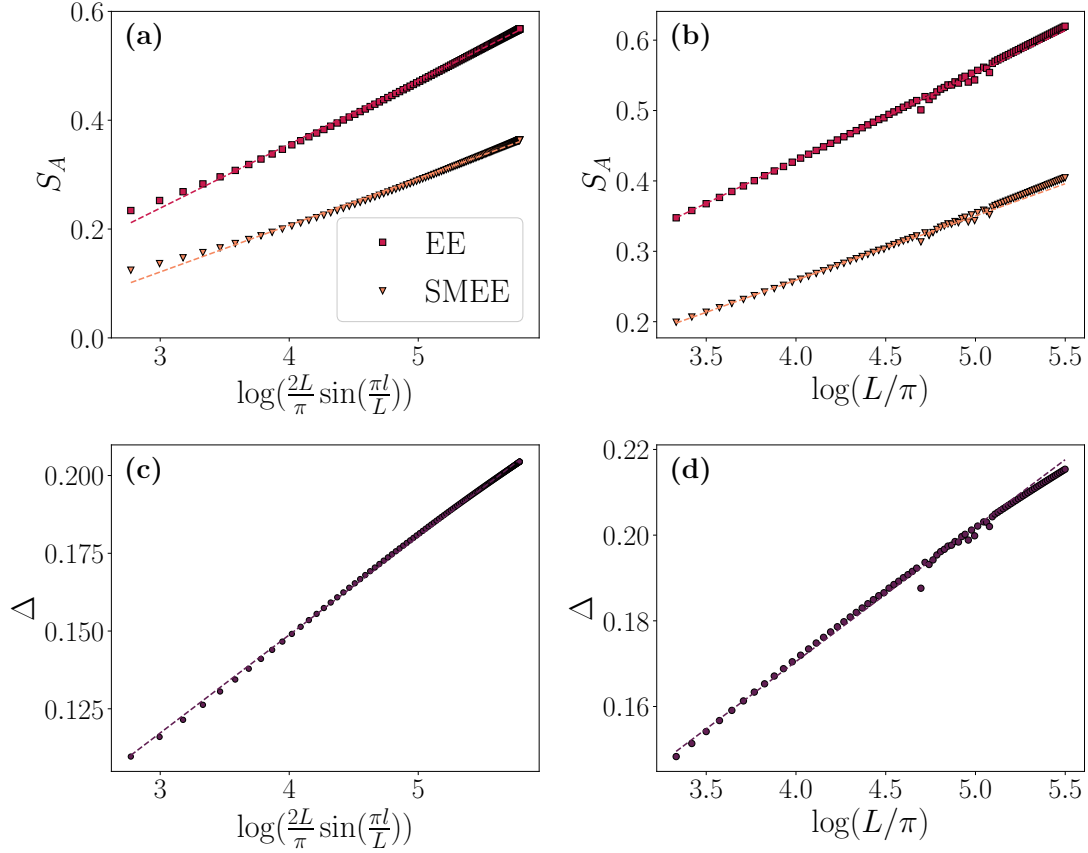
Figure 5: Entanglement entropy (EE) and Stabilizer-minimized Entanglement Entropy (SMEE) in Tricritical Ising point. For **(a)**, **(c)** data are shown for a fixed length of the system $L = 512$, varying the size of the partitions A, B ($\ell_A = l$, $\ell_B = L - l$) from $l = 8$ to $l = 256$. For **(b)**, **(d)** data are presented for varying total system lengths L with fixed, equally sized partitions A and B (where $\ell_A = \ell_B = L/2$). **(a)**, **(b)**: EE and CMEE scaling with size. While both follow the expected logarithmic trend, CMEE features a distinct prefactor. Dashed lines represent the linear fits. **(b)**, **(d)**: The gain Δ scales logarithmically with size at the TCI point. The dashed line represent the linear fit.

tem size as Local Clifford Disentanglable (LCD). What radically changes from nLCD states is the non-local magic. As shown in Fig. 4a, $m_2^{\chi=2} \sim m_2$, which implies that the magic of the state can be almost entirely removed by local operation. In this case, disentangling via Clifford operations is anticipated to be particularly effective. Our results confirm these expectations. Furthermore, the distinction between nLCD and LCD conformal field theories can be understood through the mSRE of their corresponding states. In Fig. 2b, we see that in XXZ model $L_{AB} > 0$ within the critical phase. In contrast, Fig. 4b (for system size $L = 64$) and Fig. 4d (for system size $L = 128$) show that $L_{AB} < 0$ at $\lambda_{TCI} = 0.428$. As previously discussed in Sec. 2.3, we expected a more efficient Stabilizer disentangling procedure in the latter case, and our results confirm the prediction.

6 On the origin of efficient stabilizer disentangling: cluster Ising models

While negative mSRE provides an intuitive way to understand why certain states are subjected to more efficient stabilizer disentangling than others, it is unable to provide clear information about the functional form, nor the origin of such a mechanism. Here, we show that both aspects can be addressed using Cluster Ising models as testing ground.

6.0.1 Non-local disentangling transformation as a Clifford operation

A key aspect of the cluster Ising models defined above is that, at their critical points, their ground states can be exactly mapped onto direct sums of lattice field theories. This fact, amply discussed in Ref. [30], can be understood in two ways. The first one is to note, as in Ref. [30], that the model free energy feature exact periodicity. The second one, more intuitive, is to re-write the model Hamiltonian in terms of complex fermions $c_j = \left(\prod_{i=1}^{j-1} \sigma_j^z\right)\sigma_j^-$, $c_j^\dagger = \left(\prod_{i=1}^{j-1} \sigma_j^z\right)\sigma_j^+$ (where $\sigma_j^\pm = \sigma_j^x \pm \sigma_j^y$) so that Eq. 22 becomes

$$H_3 = \sum_{i=1}^{L}(c_j^\dagger - c_j)(c_{j+2}^\dagger + c_{j+2}) + h\sum_{j=1}^{L}(c_j^\dagger + c_j)(c_{j+1}^\dagger - c_{j+1}) \,.$$

By Fourier transforming the fermionic operators and applying a Bogoliubov transformation $b_k = u_k \gamma_k + i v_k \gamma_k^\dagger$ where $u_k = \frac{1}{\sqrt{2}}\sqrt{1 + \frac{\epsilon_k}{\Lambda_k}}$, $v_k = -\frac{1}{\sqrt{2}}\sin\delta_k\sqrt{1 - \frac{\epsilon_k}{\Lambda_k}}$ and

$$\epsilon_k = \cos(\frac{4\pi k}{L}) - h\cos(\frac{2\pi k}{L}) \,,$$

$$\delta_k = \sin(\frac{4\pi k}{L}) + h\sin(\frac{2\pi k}{L}) \,,$$

and, finally, $\Lambda_k = \sqrt{1 + h^2 - 2h\cos(\frac{6\pi k}{L})}$, the Hamiltonian becomes

$$H_3 = 2\sum_{k=1}^{L}\Lambda_k\left(\gamma_k^\dagger\gamma_k - \frac{1}{2}\right) \,. \tag{25}$$

From this form, by choosing $M = \frac{L}{3}$ and splitting the summation into three separate terms, we express the Hamiltonian as

$$H = \sum_{s=1}^{3}H_{\text{Ising}}^s \tag{26}$$

thanks to the fact that by inserting M in Λ_k the dispersion relation of the Ising model is retrieved. An analogous computation can be carried out for the Hamiltonian of Eq. 20, where the absence of nearest-neighbour interaction in the y-directionaligns the final dispersion relation with that of the Ising model when $M = L/2$.

   This shows how, at the critical point, the system Hamiltonian can be expressed as a sum of two or three commuting terms, acting on distinct sublattices (up to bundary terms). Each eigenstate can then be mapped onto a direct product of wave functions leaving on the distinct sublattices. This transformation is composed of sequences of SWAP gates, and it thus a Clifford operation.

   This implies that, for partition sizes of $L/2$ and $L/3, 2L/3$ respectively, the two models will feature an SMEE resembling exactly that of an Ising model of effective size $L/2$ and $L/3$. Under the assumption that the local minimization procedure we utilize will return that (an

assumption that we will scrutinize in detail later), this consideration immediately lends itself to the following predictions: *i)* for $\ell < L/p$, SMEE will scale logarithmically, with an effective central charge that is 1/2 or 1/3 of the original one; *ii)* exactly at L/p, the SMEE will vanish; *iii)* the same patter will be repeated for all partitions, up to boundary and convergence effects. Moreover, we note that mutual SRE in real space is going to be negative for these cases: this can be seen by noticing that the original transformation can be seen as a correlation acting non-trivially in A and B irrespectively of their distances.

Below, we scrutinize the predictions above against numerical computations.

6.1 Magic scaling in cluster Ising models and stabilizer disentangling

Since it is possible to partially disentangle the critical ground state of cluster Ising models with a global Clifford operation, the question we address here is: can this operation be retrieved via local stabilizer disentangling?

It is not automatic that local stabilizer disentangling would be able to find the duality transformation described above. Indeed, the procedure could in principle get stuck into some local minima (since, ultimately, it is made to optimize entanglement locally), and be unable to retrieve the fact that part of the chain can completely decouple from the other. One would then need a Monte Carlo-like procedure to obtain the disentangling operation.

In order to have a qualitative picture of this, in Fig. 6, we depict the EE and SMEE for the critical point. One can observe that, differently from all previous cases, there is a strong sweep dependence here: few sweeps systematically overestimate the SMEE.

Most importantly, once converged, the data are perfectly consistent with the observation above: there is a perfect disentangling at $l = L/2$, signaling that simple local Clifford disentangling is able to capture the duality property described above. We note that this is not happening for arbitrary parameters across the transition line: for instance, at $D = 0.1$, full disentangling does not take place, as exemplified in Fig. 7.
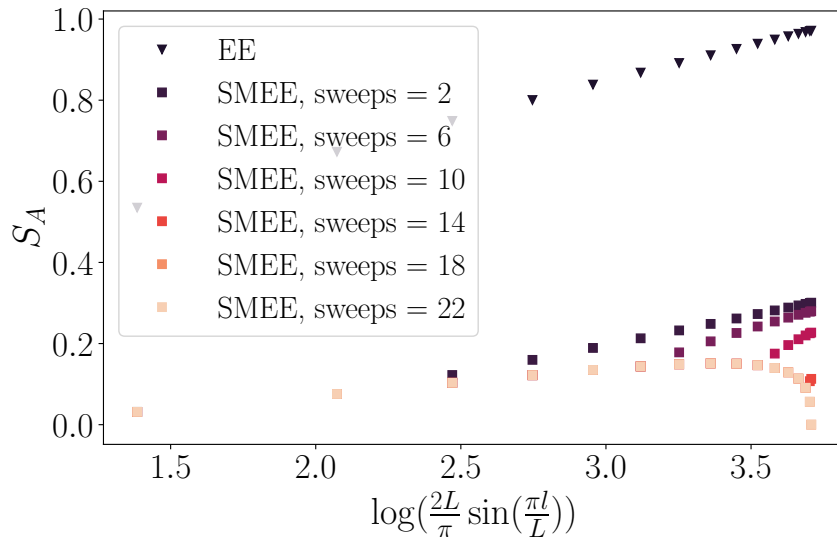
Figure 6: Entanglement entropy (EE) and Stabilizer-minimized Entanglement Entropy (SMEE) at the critical point of Eq. 20. Data are obtained for a fixed length of the system $L = 64$, varying the size of the partitions A, B ($\ell_A = l$, $\ell_B = L - Sl$) from $l = 2$ to $l = 32$.
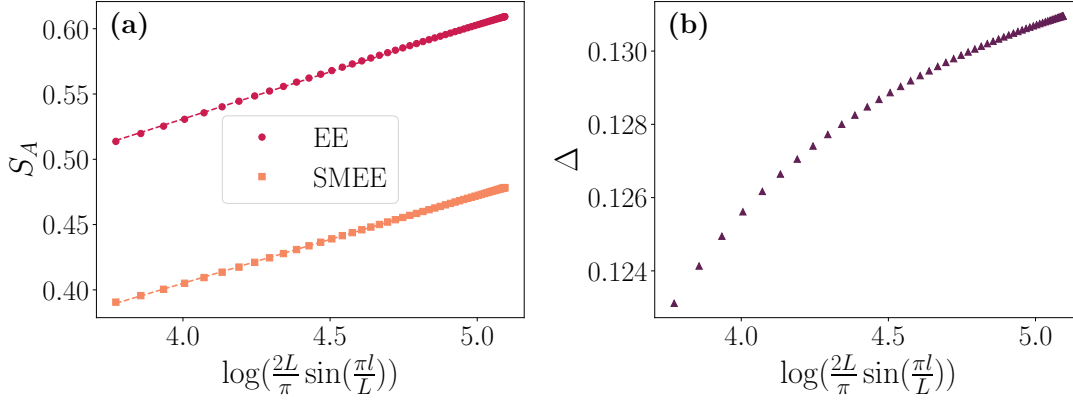
Figure 7: Stabilizer disentangling at the critical point ($D = 0.1$, $h = 0.9$) of Cluster Ising model in Eq. 21. Data are obtained for a fixed length of the system $L = 256$, varying the size of the partitions A, B ($\ell_A = l$, $\ell_B = L - l$) from $l = 20$ to $l = 128$. **(a)** Scaling of Entanglement Entropy (EE) and Stabilizer-Minimized Entanglement Entropy (SMEE) with subsystem size ℓ. Dashed lines represent the fitted curves, with both curves sharing the same slope. **(b)** Scaling of Entropy gain Δ with subsystem size ℓ. **(b)** Scaling of entropy gain Δ. It exhibits sublogarithmic scaling; however, due to the very small scale on the y-axis.
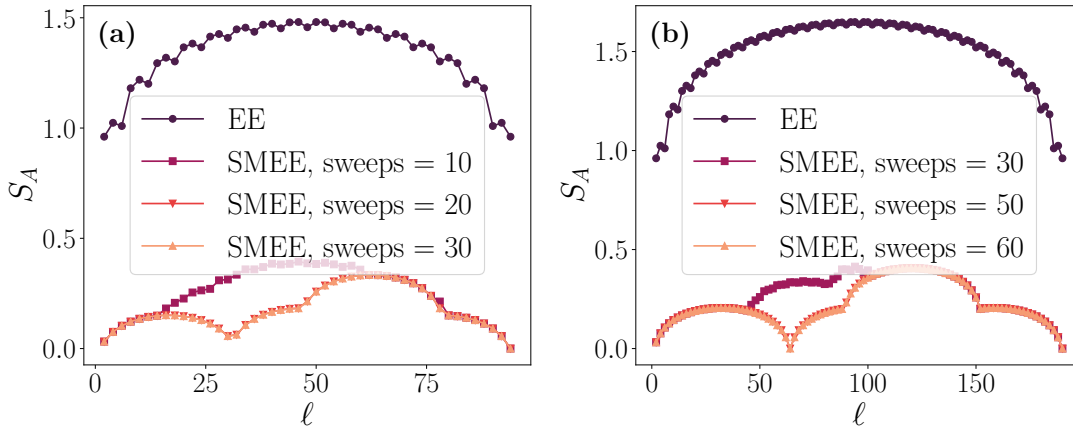
Figure 8: Entanglement entropy (EE) and Stabilizer-minimized Entanglement Entropy (SMEE) at the critical point of Cluster Ising model in Eq. 22. **(a)** System size $L = 96$; **(b)** System size $L = 192$.

To further corroborate the efficiency of disentangling, we consider the Cluster Ising model in Eq. 22, which features instead a tripartite unit cell over duality. The corresponding results are depicted in Fig. 8. As can be seen in both plots (representing different volumes), the SMEE is a strongly non-monotonous function of the partition size. In particular, it becomes compatible with 0 at $L/3$, in perfect agreement with the exact disentanglement expected at convergence. Interesting, we are unable to see the same behavior at $2L/3$ at large volumes (we observe it only at $L = 24$): we believe this may be due to the fact that the transformation has large (3-site) support, so a minimization based on two-body gates only may not be enough for full disentangling.

As a final confirmation of our theory, in Fig. 9, we plot the SMEE obtained from the cluster Ising models, with the EE and SMEE of the of the Ising model defined on a third of its volume. We observe an almost perfect quantitative agreementn (no adjustable parameters) between the Ising SMEE and the Cluster Ising SMEE of a larger system, corroborating the fact that local Clifford circuits are indeed able to fully capture the model duality at the full wave function level. Moreover, in the cluster Ising model at criticality, $L_{AB} < 0$. This completes the picture we proposed: for CAMPS to showcase systematic improvement over MPS, a negative mSRE and the presence of non-local stabilizer information is key.

7 Conclusions

We have scrutinized the possibility of systematically disentangle ground states of quantum spin chains using local Clifford operations. From the complexity viewpoint, the procedure we described can be thought of as a lowering of entanglement complexity, while keeping magic complexity invariant. More specifically, the expectation value of any observable with low Pauli weight can be efficiently computed on an MPS with lower bond dimension, thus reducing the computational cost.

Within this framework, we have shown how the large corner of the Hilbert space comprising matrix product states features very diverse sets. Some states are local-Clifford disentanglable, that is, once system size increases, the bond dimension required to describe a given state is parametrically smaller than that of an MPS. This implies that, to simulate such states, hybrid methods such as Clifford-augmented MPS are systematically better than traditional MPS (they trade a systematic cost for a gain that improves with size). At specific points in parameter space, such states can even become fully disentanglable. Another class of states is instead made of states that cannot be Clifford disentangled apart from a constant contribution.
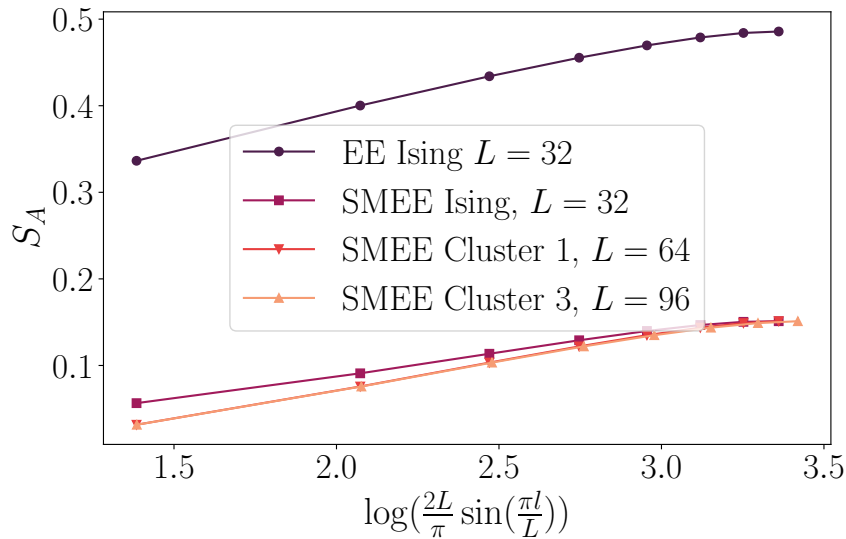
Figure 9: Comparison of Entanglement Entropy in Ising and Cluster Ising models after Stabilizer Disentangling. Data are shown for a fixed system size L, indicated in the legend, varying the sizes of the partition A, B ($\ell_A = l$, $\ell_B = L - l$) from $l = 2$ to $l = 16$. Both EE and SMEE exhibit the expected logarithmic scaling behavior, and, for different models, SMEEs are compatible.

We have elucidated the origin of such a mechanism utilizing mutual Stabilizer Renyi entropies. Despite not being measures of magic for mixed states, the latter still serve as a quantifier of localization in stabilizer space. Combining qualitative reasoning with exactly solvable examples, we have argued that the key feature for a state to be stabilizer disentangled resides in the sign of the mutual Stabilizer Renyi entropy: if negative, it captures the fact that there are non-local correlations (entanglement) that can be systematically diminished via the application of Clifford operations only.

Our work paves the way to a series of extensions, and leaves open questions. First of all, it calls for a deeper (field) theoretical understanding of mSRE. While those have already been shown to be superior to full state magic in determining critical behavior in a number of cases, they still lack a generic relation to continuum description. Based on the results reported above, understanding the latter would be crucial to better identify the relation between the hybrid complexity classes defined above and physical properties - and, ultimately, defined for which classes of phenomena lowering complexity with CAMPS can work. Similarly, it would be important to understand the role of mSRE in out of equilibrium dynamics. The fact that in those scenarios, improved performances of CAMPS have been so far less promising that for ground states, may be explained by the fact that in such situations, it is very unlikely to observe states with negative mSRE.

At a broader theoretical level, it would be extremely interesting to formulate measures of computational complexity that are hybrid between entanglement and magic - and can thus lower bound the complexity of representing a state using either tensor networks or Pauli tableaus, and establish connections between tensor networks are alternative approaches [68]. Understanding such hybrid complexity would be crucial to address the capability of other classes of Clifford-augmented tensor networks, including tree-tensor and projected-entangled paired states, that are better suited to represent higher-dimensional states. Our proposal to attack this targeting participation entropy in stabilizer subspace could be checked in all such tensor network settings utilizing Pauli-Markov chains, and may stimulate the search for alternative quantities to define hybrid complexity. Finally, it may also be interesting to explore alternatives to systematic disentangling, e.g., including an element of stochasticity, to further decrease entanglement.

ACKNOWLEDGMENTS

We thank B. Béri, R. Fazio, G. Fux, A. Hamma, T. Haug, R. Nehra, M. Qin and H. Timsina for inspiring discussions.

Funding information   P.S.T. acknowledges funding by the Deutsche Forschungsgemeinschaft (DFG, German Research Foundation) under Germany's Excellence Strategy – EXC-2111 – 390814868. M.D. was partly supported by the QUANTERA DYNAMITE PCI2022-132919, by the EU-Flagship programme Pasquans2, by the PNRR MUR project PE0000023-NQSTI, by the PRIN programme (project CoQuS), by the MIUR Programme FARE (MEPH), and by the ERC Grant WaveNets.

Note added: after this work appeared on arxiv, a related manuscript by Fan and coworked was posted (arXiv:2411.12683). While models and protocol differ, their conclusions on different performances on CAMPS wave functions are in agreement with our findings.
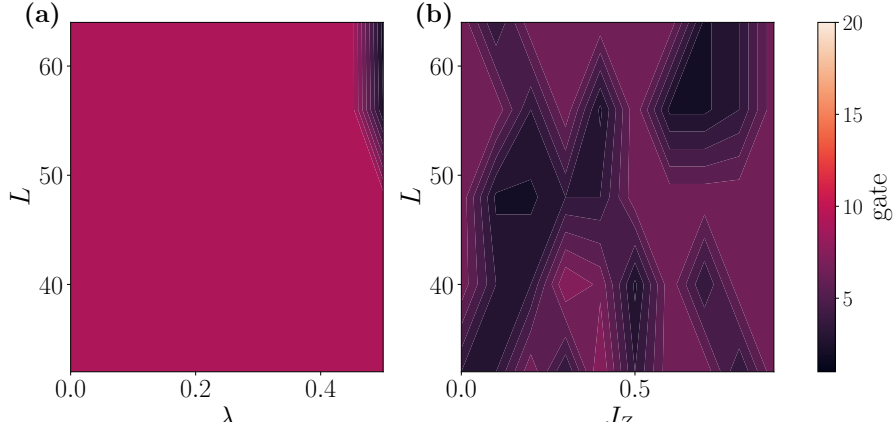
Figure 10: Illustration of gate selection during the first sweep of the Stabilizer Disentangling protocol, across various parameters and system sizes. The gate selected in the process is uniform in the bulk of the chain. **(a)** Results for the TCI model; **(b)** Results for the XXZ model.

A Gate choosing

In this section, we provide detailed descriptions of the gate selection process employed by the Stabilizer Disentangling protocol. Fig. 10 shows the results for two distinct models: the Tricritical Ising model in Fig. 10a and the XXZ model in Fig. 10b. In both cases, onvergence was independent of the number of sweeps, with a single sweep being sufficient to achieve the minimum SMEE. Interestingly, even without constraints on gate selection, the disentangling protocol uniformly selects the same gate in the bulk of the chain, consistent with expectations based on the homogeneous structure of the ground states. For this reasons, the single gate showed in the colormaps in Fig. 10 corresponds to the one selected in the bulk of the chains during the first sweep of the minimization. In Fig. 10a we observe that for the Tricritical Ising model case, where groundstates belong to the LCD of the Hilber space (both for critical point and area-law phases), gate selection remains independent of system size L and parameter λ. In contrast, for XXZ model, whose groundstates fall within the nLCD sector, the gate selections shows some variations across different values of the parameter J_z in the critical phase. Although the gate choice is not identical for each combination of J_z and L, the protocol still explores only a limited subset of $\tilde{C}_2$ gates for minimization.

B Estimation of critical point in Cluster Ising models

We consider the Hamiltonian in Eq. 21 and estimate the critical value of the parameter h for a fixed $D = 0.1$ by analyzing the system's entanglement entropy. Our results are depicted in Fig. 11. On the left panel, we show the entropy divided by $\log(L)$ for various volumes. This indicates rather sharply that, in the vicinity of 0.9, a critical scaling is observed (another regime that resemble criticality also emerges at larger h, but we do not consider it here).

In order to estimate the position of the critical point, we utilize a fine grid in parameter space, and plot the position of the maximum versus inverse volume in the right panel. We observe a trend that is compatible with linear scaling, and extract $h_c = 0.903 \pm 0.001$.
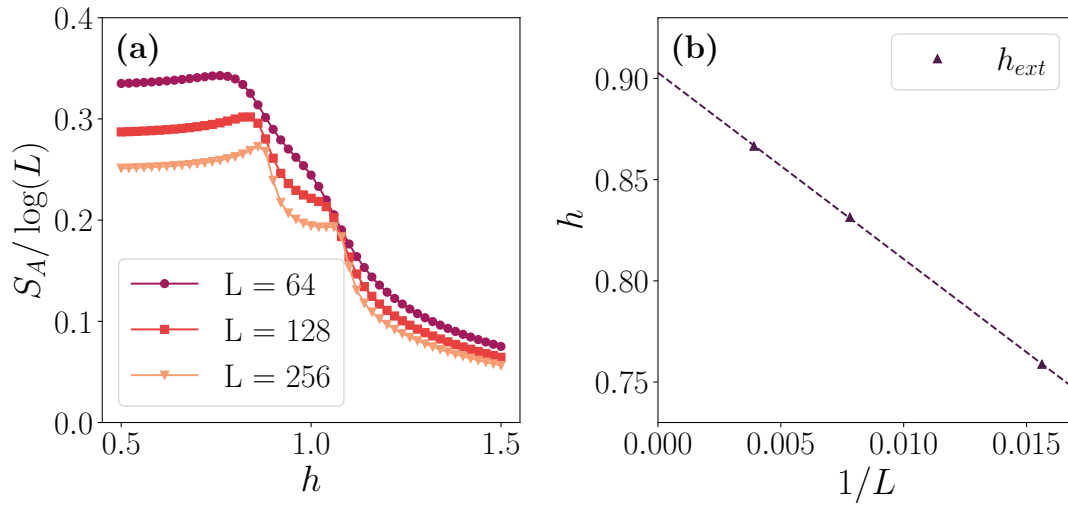
Figure 11: Estimation of the critical point of the Hamiltonian in Eq. 21, for fixed parameter $D = 0.1$. **(a)**: Scaling of Entanglement Entropy (EE) with parameter h for various system sizes. **(b)** Size scaling for the estimation of the critical point h_c. The points correspond to the positions of the peak in panel (a), the dashed line represnts the linear fit. The estimated intercept is $h_c = 0.903 \pm 0.001$.

References

[1] S. R. White, *Density-matrix algorithms for quantum renormalization groups*, Physical review b **48**(14), 10345 (1993).

[2] J. Dukelsky, M. Martín-Delgado, T. Nishino and G. Sierra, *Equivalence of the variational matrix product method and the density matrix renormalization group applied to spin chains*, Europhysics Letters (EPL) **43**(4), 457 (1998).

[3] F. Verstraete, V. Murg and J. I. Cirac, *Matrix product states, projected entangled pair states, and variational renormalization group methods for quantum spin systems*, Advances in physics **57**(2), 143 (2008).

[4] U. Schollwöck, *The density-matrix renormalization group in the age of matrix product states*, Annals of physics **326**(1), 96 (2011).

[5] R. Orús, *A practical introduction to tensor networks: Matrix product states and projected entangled pair states*, Annals of Physics **349**, 117 (2014), doi:https://doi.org/10.1016/j.aop.2014.06.013.

[6] S. Montangero, E. Montangero and Evenson, *Introduction to tensor network methods*, Springer (2018).

[7] S.-J. Ran, E. Tirrito, C. Peng, X. Chen, L. Tagliacozzo, G. Su and M. Lewenstein, *Tensor network contractions: methods and applications to quantum many-body systems*, Springer Nature (2020).

[8] F. Verstraete, T. Nishino, U. Schollwöck, M. C. Bañuls, G. K. Chan and M. E. Stoudenmire, *Density matrix renormalization group, 30 years on*, Nature Reviews Physics **5**(5), 273 (2023).

[9] G. Vidal, *Class of quantum many-body states that can be efficiently simulated*, Physical review letters **101**(11), 110501 (2008).

[10] T. Felser, S. Notarnicola and S. Montangero, *Efficient tensor network ansatz for high-dimensional quantum many-body problems*, Physical Review Letters **126**(17), 170603 (2021).

[11] X. Qian and M. Qin, *From tree tensor network to multiscale entanglement renormalization ansatz*, Physical Review B **105**(20) (2022), doi:10.1103/physrevb.105.205102.

[12] X. Qian and M. Qin, *Augmenting density matrix renormalization group with disentanglers*, Chinese Physics Letters **40**(5), 057102 (2023).

[13] D. Gottesman, *Stabilizer codes and quantum error correction*, California Institute of Technology (1997).

[14] S. Bravyi and A. Kitaev, *Universal quantum computation with ideal Clifford gates and noisy ancillas*, Phys. Rev. A **71**, 022316 (2005), doi:10.1103/PhysRevA.71.022316.

[15] E. T. Campbell, B. M. Terhal and C. Vuillot, *Roads towards fault-tolerant universal quantum computation*, Nature **549**(7671), 172 (2017), doi:10.1038/nature23460.

[16] X. Qian, J. Huang and M. Qin, *Augmenting density matrix renormalization group with clifford circuits*, arXiv preprint arXiv:2405.09217 (2024).

[17] S. Masot-Llima and A. Garcia-Saez, *Stabilizer tensor networks: universal quantum simulator on a basis of stabilizer states* (2024), 2403.08724.

[18] A. F. Mello, A. Santini and M. Collura, *Hybrid stabilizer matrix product operator*, Physical Review Letters **133**(15), 150604 (2024).

[19] G. Lami, T. Haug and J. De Nardis, *Quantum state designs with clifford enhanced matrix product states*, arXiv preprint arXiv:2404.18751 (2024).

[20] M. Frau, P. Tarabunga, M. Collura, M. Dalmonte and E. Tirrito, *Nonstabilizerness versus entanglement in matrix product states*, Physical Review B **110**(4), 045101 (2024).

[21] X. Qian, J. Huang and M. Qin, *Augmenting finite temperature tensor network with clifford circuits*, arXiv preprint arXiv:2410.15709 (2024).

[22] A. F. Mello, A. Santini, G. Lami, J. De Nardis and M. Collura, *Clifford dressed time-dependent variational principle*, arXiv preprint arXiv:2407.01692 (2024).

[23] X. Qian, J. Huang and M. Qin, *Clifford circuits augmented time-dependent variational principle*, arXiv preprint arXiv:2407.03202 (2024).

[24] P. Francesco, P. Mathieu and D. Sénéchal, *Conformal field theory*, Springer Science & Business Media (2012).

[25] C. Holzhey, F. Larsen and F. Wilczek, *Geometric and renormalized entropy in conformal field theory*, Nuclear physics b **424**(3), 443 (1994).

[26] P. Calabrese and J. Cardy, *Entanglement entropy and quantum field theory*, Journal of Statistical Mechanics: Theory and Experiment **2004**(06), P06002 (2004), doi:10.1088/1742-5468/2004/06/p06002.

[27] L. Leone, S. F. E. Oliviero and A. Hamma, *Stabilizer rényi entropy*, Phys. Rev. Lett. **128**, 050402 (2022), doi:10.1103/PhysRevLett.128.050402.

[28] T. Haug and L. Piroli, *Stabilizer entropies and nonstabilizerness monotones*, Quantum **7**, 1092 (2023), doi:10.22331/q-2023-08-28-1092.

[29] P. S. Tarabunga, E. Tirrito, T. Chanda and M. Dalmonte, *Many-body magic via pauli-markov chains—from criticality to gauge theories*, PRX Quantum **4**, 040317 (2023), doi:10.1103/PRXQuantum.4.040317.

[30] P. Smacchia, L. Amico, P. Facchi, R. Fazio, G. Florio, S. Pascazio and V. Vedral, *Statistical mechanics of the cluster ising model*, Phys. Rev. A **84**, 022304 (2011), doi:10.1103/PhysRevA.84.022304.

[31] S. Aaronson and D. Gottesman, *Improved simulation of stabilizer circuits*, Phys. Rev. A **70**, 052328 (2004), doi:10.1103/PhysRevA.70.052328.

[32] Z.-W. Liu and A. Winter, *Many-body quantum magic*, PRX Quantum **3**(2), 020333 (2022), doi:10.1103/PRXQuantum.3.020333.

[33] M. Howard and E. Campbell, *Application of a resource theory for magic states to fault-tolerant quantum computing*, Phys. Rev. Lett. **118**, 090501 (2017), doi:10.1103/PhysRevLett.118.090501.

[34] A. Heimendahl, F. Montealegre-Mora, F. Vallentin and D. Gross, *Stabilizer extent is not multiplicative*, Quantum **5**, 400 (2021), doi:10.22331/q-2021-02-24-400.

[35] V. Veitch, S. H. Mousavian, D. Gottesman and J. Emerson, *The resource theory of stabilizer quantum computation*, New Journal of Physics **16**(1), 013009 (2014), doi:10.1088/1367-2630/16/1/013009.

[36] M. Beverland, E. Campbell, M. Howard and V. Kliuchnikov, *Lower bounds on the non-clifford resources for quantum computations*, Quantum Science and Technology **5**(3), 035009 (2020).

[37] X. Turkeshi, E. Tirrito and P. Sierant, *Magic spreading in random quantum circuits*, arXiv preprint arXiv:2407.03929 (2024).

[38] P. S. Tarabunga, M. Frau, T. Haug, E. Tirrito and L. Piroli, *A nonstabilizerness monotone from stabilizerness asymmetry* (2024), 2411.05766.

[39] T. Haug and M. Kim, *Scalable measures of magic resource for quantum computers*, PRX Quantum **4**, 010301 (2023), doi:10.1103/PRXQuantum.4.010301.

[40] D. Bluvstein, S. J. Evered, A. A. Geim, S. H. Li, H. Zhou, T. Manovitz, S. Ebadi, M. Cain, M. Kalinowski, D. Hangleiter *et al.*, *Logical quantum processor based on reconfigurable atom arrays*, Nature **626**(7997), 58 (2024).

[41] P. Niroula, C. D. White, Q. Wang, S. Johri, D. Zhu, C. Monroe, C. Noel and M. J. Gullans, *Phase transition in magic with random quantum circuits*, Nature Physics pp. 1–7 (2024).

[42] S. F. E. Oliviero, L. Leone, A. Hamma and S. Lloyd, *Measuring magic on a quantum processor*, npj Quantum Information **8**(1) (2022), doi:10.1038/s41534-022-00666-5.

[43] E. Tirrito, P. S. Tarabunga, G. Lami, T. Chanda, L. Leone, S. F. E. Oliviero, M. Dalmonte, M. Collura and A. Hamma, *Quantifying nonstabilizerness through entanglement spectrum flatness*, Physical Review A **109**(4) (2024), doi:10.1103/physreva.109.l040401.

[44] T. Haug and L. Piroli, *Quantifying nonstabilizerness of matrix product states*, Phys. Rev. B **107**, 035148 (2023), doi:10.1103/PhysRevB.107.035148.

[45] G. Lami and M. Collura, *Nonstabilizerness via perfect pauli sampling of matrix product states*, Phys. Rev. Lett. **131**, 180401 (2023), doi:10.1103/PhysRevLett.131.180401.

[46] P. S. Tarabunga, E. Tirrito, M. C. Bañuls and M. Dalmonte, *Nonstabilizerness via matrix product states in the pauli basis*, Phys. Rev. Lett. **133**, 010601 (2024), doi:10.1103/PhysRevLett.133.010601.

[47] P. S. Tarabunga and C. Castelnovo, *Magic in generalized rokhsar-kivelson wavefunctions*, Quantum **8**, 1347 (2024), doi:10.22331/q-2024-05-14-1347.

[48] Z. Liu and B. K. Clark, *Non-equilibrium quantum monte carlo algorithm for stabilizer rényi entropy in spin systems*, arXiv:2405.19577 (2024).

[49] P. S. Tarabunga, *Critical behaviors of non-stabilizerness in quantum spin chains*, Quantum **8**, 1413 (2024).

[50] J. A. M. López and P. Kos, *Exact solution of long-range stabilizer renyi entropy in the dual-unitary xxz model*, arXiv:2405.04448 (2024).

[51] P. S. Tarabunga and E. Tirrito, *Magic transition in measurement-only circuits*, arXiv:2407.15939 (2024).

[52] X. Turkeshi, A. Dymarsky and P. Sierant, *Pauli spectrum and magic of typical quantum many-body states* (2023), 2312.11631.

[53] U. Schollwöck, *The density-matrix renormalization group in the age of matrix product states*, Annals of Physics **326**(1), 96–192 (2011), doi:10.1016/j.aop.2010.09.012.

[54] E. M. Stoudenmire and S. R. White, *Minimally entangled typical thermal state algorithms*, New Journal of Physics **12**(5), 055026 (2010), doi:10.1088/1367-2630/12/5/055026.

[55] A. J. Ferris and G. Vidal, *Perfect sampling with unitary tensor networks*, Phys. Rev. B **85**, 165146 (2012), doi:10.1103/PhysRevB.85.165146.

[56] M. Fishman, S. R. White and E. M. Stoudenmire, *The ITensor Software Library for Tensor Network Calculations*, SciPost Phys. Codebases p. 4 (2022), doi:10.21468/SciPostPhysCodeb.4.

[57] M. Fishman, S. R. White and E. M. Stoudenmire, *Codebase release 0.3 for ITensor*, SciPost Phys. Codebases pp. 4–r0.3 (2022), doi:10.21468/SciPostPhysCodeb.4-r0.3.

[58] P. Calabrese and J. Cardy, *Entanglement entropy and conformal field theory*, Journal of physics a: mathematical and theoretical **42**(50), 504005 (2009).

[59] A. O. Gogolin, A. A. Nersesyan and A. M. Tsvelik, *Bosonization and strongly correlated systems*, Cambridge university press (2004).

[60] E. O'Brien and P. Fendley, *Lattice supersymmetry and order-disorder coexistence in the tricritical ising model*, Phys. Rev. Lett. **120**, 206403 (2018), doi:10.1103/PhysRevLett.120.206403.

[61] S. O. Skrøvseth and S. D. Bartlett, *Phase transitions and localizable entanglement in cluster-state spin chains with ising couplings and local fields*, Phys. Rev. A **80**, 022316 (2009), doi:10.1103/PhysRevA.80.022316.

[62] A. C. Doherty and S. D. Bartlett, *Identifying phases of quantum many-body systems that are universal for quantum computation*, Phys. Rev. Lett. **103**, 020506 (2009), doi:10.1103/PhysRevLett.103.020506.

[63] J. K. Pachos and M. B. Plenio, *Three-spin interactions in optical lattices and criticality in cluster hamiltonians*, Phys. Rev. Lett. **93**, 056402 (2004), doi:10.1103/PhysRevLett.93.056402.

[64] R. Raussendorf, D. E. Browne and H. J. Briegel, *Measurement-based quantum computation on cluster states*, Phys. Rev. A **68**, 022312 (2003), doi:10.1103/PhysRevA.68.022312.

[65] F. Verstraete and J. I. Cirac, *Valence-bond states for quantum computation*, Phys. Rev. A **70**, 060302 (2004), doi:10.1103/PhysRevA.70.060302.

[66] J. I. Cirac, D. Pérez-García, N. Schuch and F. Verstraete, *Matrix product states and projected entangled pair states: Concepts, symmetries, theorems*, Rev. Mod. Phys. **93**, 045003 (2021), doi:10.1103/RevModPhys.93.045003.

[67] G. E. Fux, B. Béri, R. Fazio and E. Tirrito, *Disentangling unitary dynamics with classically simulable quantum circuits*, arXiv preprint arXiv:2410.09001 (2024).

[68] A. Angrisani, A. Schmidhuber, M. S. Rudolph, M. Cerezo, Z. Holmes and H.-Y. Huang, *Classically estimating observables of noiseless quantum circuits*, arXiv preprint arXiv:2409.01706 (2024).